Investigation of a plane mixing layer-wake interaction by means of two $2D$ PIV planes and of POD

C. Braud, D. Heitz*, P. Braud, G.Arroyo* and J. Delville

L.E.A. (Laboratoire d'Etudes Aérodynamiques), UMR CNRS 6609,
CEAT 43 Route de l'Aérodrome, F 86036 Poitiers - France
*CEMAGREF,
17, avenue de Cucillé, F35044 Rennes cedex - France
E-mail : caroline.braud@cemagref.fr

Abstract

The strong interaction between turbulent structures arising from a plane mixing layer impinging a circular cylinder is studied using P.I.V. and analysed by means of the Proper Orthogonal Decomposition (P.O.D. [Lumley(1967*b*)]).

Experiments are performed in the wake of a circular cylinder placed across an air/air 2D plane turbulent mixing layer (velocity ratio r=0.65). The cylinder axis is normal to the splitting plate (Fig. 1-a). The Reynolds number, based on the averaged velocity of the mixing layer is R_{em}=7920 (U_m=14.85,D=8 mm). The cylinder is placed so that δ_ω, the local vorticity thickness of the mixing layer, is equal to the diameter of the cylinder D [Heitz(1999)]. To study this complex 3D configuration, a POD approach is proposed. The three spatial directions being strongly inhomogeneous and no experimental way being presently available to get a fully 3D, three components instantaneous description of the flow, a snapshot POD approach [Sirovish(1989)] is not possible and a 'classical' POD [Lumley(1967*b*)] has to be used.

Experiments are carried out to supply the correlation tensor, necessary for applying this last POD approach. A two 2D-plane PIV is set-up. The two PIV planes are arranged perpendicularly to the splitting plate and are parallel (Fig. 1-b). Measurements are performed for a set of spanwise separations between the PIV-planes (over a mesh of 21 planes locations). The measurements are performed over a volume $L_x \times L_y \times L_z$=$10.5 \times 7.75 \times 10.5\ {\delta_\omega}^3$. Due to the inhomogeneity in this direction, all the combinations of the two planes over this mesh, are to be considered, leading to a set of 231 configurations. By this procedure, the full correlation tensor $R_{ij}(X,X')$ where X=(x,y,z), is supplied for the longitudinal and vertical velocity components $(i,j$=1,2) only. The POD eigenfunctions $\Phi_u^{(n)}(X)$ and $\Phi_v^{(n)}(X)$ are then obtained by solving the following integral eigenvalue problem:

$$\sum_{j=1}^{2} \int_\Omega R_{ij}(X,X')\Phi_j^{(n)}(X')\,dX' = \lambda^{(n)}\Phi_i^{(n)}(X) \qquad (1)$$

The contribution of the third velocity component $\Phi_w^{(n)}(X)$ is obtained *a posteriori* by considering the continuity equation.

In this paper, after a quick review of the industrial and fundamental aspects of this flow configuration, the experimental procedure is described. In a preliminary validation analysis, the one point statistics obtained from PIV measurements are compared to that obtained, in a comparable flow configuration, [Heitz(1999)] by means of hot-wire anemometry. Then the practical aspects of POD calculation, related to the resolution of a very large size eigenvalue problem are addressed. Finally the flow organisation issued from the POD approach is obtained (Fig. 1-c). The resulting structures show that some kind of a dislocation process is involved that is comparable to the one described for example in [Williamson(1989)].

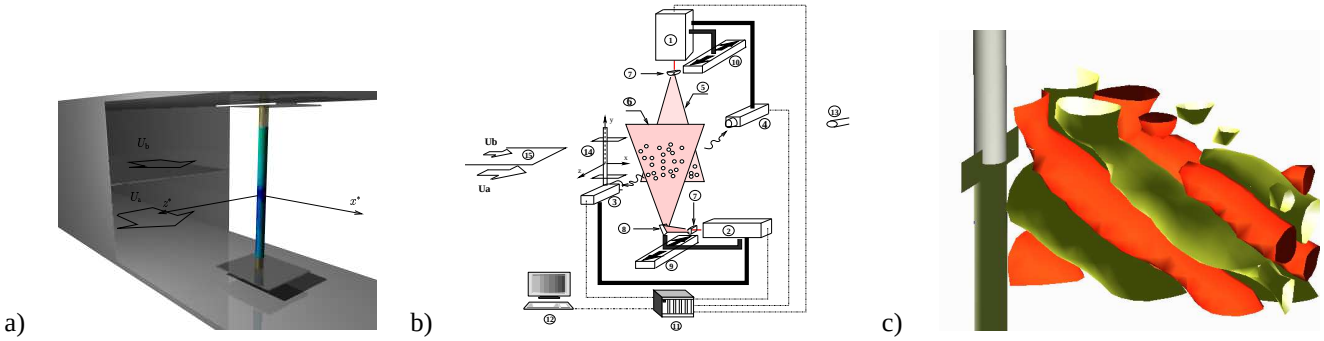

Figure 1: a) Flow configuration ; b) Experimental setup (see Fig. 3 for details) ; c) Isocontour of the spanwise vorticity ω_z contribution of the first POD mode

1 Introduction

The interaction between a plane mixing layer and the wake of a slender body is of great interest in numerous practical configurations like heat exchangers, off-shore structures, wind- turbines, smokestacks, etc. In the present study, the motivation was to understand and control the behaviour of such a flow in devices designed for the food industry to deliver localised airflow generating a clean environment around sensitive food products. Such a technique has been developed by the Cemagref for the shielding of food products against airborne contamination. It can be applied to parts of the production lines where the products are laying on a working table or a conveyor (Fig. 2, left). One of the originalities of the technique relies in the fact that the protected area remains open to human interventions. In that context, a peculiar attention has to be paid to the perturbations induced by obstacles, like human arms, penetrating into the clean air flow from outside the protected area. As a first approach to the study of those perturbations and their consequences on pollution transfer towards the clean zone, the problem was approximated by studying the interaction between the wake of a cylinder and a plane mixing layer (Fig.2, right). The cylinder can be taken as a generic shape for the arms, while the interface between the clean and the polluted air can be considered correctly represented by a mixing layer with high speed on the clean side.

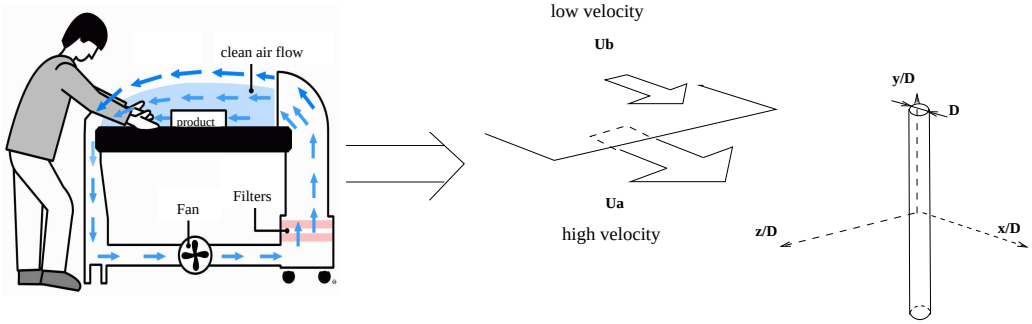

Figure 2: Going from the food industry problem to a more fundamental and generic approach

The interaction of the wake of a circular cylinder and a turbulent plane mixing layer belongs to complex flows. This kind of flow is at present not much studied. This is partly due to the fully three-dimensional organization in the near wake where experimental and numerical investigations are difficult to carry out. Nevertheless attempts have been made to understand the physical nature of the coupling between the two- and three-dimensional processes in the wake of a nominally two-dimensional cylinder [Bearman(1998)]. All of the three-dimensionalities caused by velocity shear [von Karman & Tsien(1945)], [Maull & Young(1973)], [Tavoularis *et al.*(1987)], [Woo *et al.*(1989)], diameter taper [Lewis & Gharib(1992)], wake of a cone [Gaster(1969)], local discontinuity in cylinder diameter and end conditions [Szepessy & Bearman(1992)], [Lewis & Gharib(1992)], [Gerich & Eckelmann(1982)], [Norberg(1994)] and [Williamson(1996)]) are similar in behaviour. In all of these flows, there is a spanwise variation of Strouhal frequency that is tied in with the three-dimensional vorticity dynamics. For small perturbations, cells of constant frequency shedding appear. Between these regions, the neighbouring vortices are forced to find suitable terminations linkages. [Williamson (1989)], proposed a linkage model for the spanwise dislocations. [Lewis & Gharib(1992)] investigated the wake three-dimensionality caused by a local discontinuity in the cylinder diameter (stepped cylinder). They found two kind of vortex linkage depending on the diameter ratio and on the Reynolds number. [Woo *et al.*(1989)] studied the secondary flows and vortex formation around a circular cylinder in a constant shear. In this case the boundaries of the cells of constant frequency are defined by a local accumulation of the vorticity of the oncoming flow, which is rolled up around the obstacle to form a longitudinal vortex. In our study, the mixing layer not only shows this vorticity, but also introduces a significant additional parameter, namely the instationarity of the oncoming flow.

Thus in the frame of stability analysis, it is considered that there can exist at least three oscillators, the mixing layer and the two wakes (the high velocity side wake and the low velocity side wake), each one being likely to interact on the others. The comprehension of the mechanisms involved, in particular in the near wakes of the cylinder, is important to clarify the three-dimensional organization which results from it.

Previous studies of this flow [Heitz *et al.*(1997)], [Heitz *et al.*(1998)] and [Heitz(1999)]) showed that strong interactions take place just behind the shedding body. In the near wake, a non-stationary secondary flow from the low to the high velocity side was observed, which is probably linked to the oncoming structures of the mixing layer and to shedded structures of the circular cylinder. The shedding along the span of the body breaks into cells of constant frequency due to the high and low velocity sides of the mixing layer. At the cell boundary, there is a beating of the neighbouring cells and mixing layer frequencies. The aforementioned experiments indicated that a level of organization exists in the near-wake zone of interaction.

It is our motivation here to give a description of the coherent structures in the near-wake zone of interaction.

Dealing with the experimental approach of such a problem, the **P**article **I**mage **V**elocimetry (**PIV**) is now an often used technique for analysing complex flows. While “Conventionnal” **2D PIV** provides only two velocity components in a 2D plane of the flow, stereoscopic PIV can nowadays be used to measure the third component in that plane. For both techniques, the resolution in time is strongly limited by the actual frame rates of the CCD cameras classically

used for PIV. Recently [Kahler(2000)] has performed a multiple stereo PIV (dual-plane PIV) to yield a better temporal resolution.[Kahler *et al.*(2000)] and [Hu *et al.*(2001)] have applied this technique to obtain a complete set of data needed for the analysis of complex flows. Thus, they showed that a combination of PIV measurements can be a relevant way to retrieve spatial-time correlations together with improved accuracy in vorticity measurement.

On the other hand, the **P**roper **O**rthogonal **D**ecomposition (**POD**) has proven to be a powerful tool to extract complex information from consistent sets of measurement data, allowing the extraction of coherent structures and so contributing to a relevant analysis of the behaviour of complex flows.

In this paper a two PIV planes technique, hereafter called **bi-PIV**, is used to acquire a large set of data in a wind tunnel. The flow under investigation is the complex 3D flow, *inhomogeneous in all three directions*, obtained by the interaction of a plane mixing layer and a wake (Fig. 2, right). These data are then submitted to a post-treatment (classical POD), to calculate the first POD modes. The strategy chosen to cope with the problem arising from the huge size of the correlation tensor is briefly explained.

Firstly, the flow configuration is introduced. Secondly, classical POD is formulated. Thirdly the bi-PIV experimental setup is presented. The POD kernel construction is explained in a fourth part. Finally, results are given and discussed.

2 Flow Configuration

Experiments are performed in the *R300* closed-loop wind tunnel of the **CEAT** (**C**entre d'**E**tude **A**erodynamique et **T**hermique). This wind tunnel has a square test section of 300×300 mm^2 and is 2 m long, with a contraction ratio of 10. For more details about the facility, the reader can refer to [Heitz(1999)]. Air flow, generated by a fan, passes through filters of different airloss, in order to generate two velocity levels on both sides of a thin splitter plate (U_b=11.7 m/s and U_a=18 m/s ; plate thickness=3 mm). The boundary layers on both sides of the splitter plate are fully turbulent with a momentum thickness $\theta \simeq 1$ mm. The velocity ratio between the two streams is r=0.65, with an average convective velocity $U_m=(U_a + U_b)/2$=14.85 m/s. The free stream levels of turbulence are less than 0.3%. Previous studies have shown that without the cylinder, the plane mixing layer reaches the self-similarity state, for the mean velocity profiles, 140 mm dowstream of the trailing edge of the splitter plate, with an expansion factor σ of about 48. The circular cylinder, of diameter D=8 mm, is placed 159 mm downstream of the splitter plate, so that $\delta_\omega = D$, where δ_ω is the local vorticity thickness of the mixing layer. Rectangular plates ($8D$ length and $7D$ width) are placed near the circular cylinder ends in order to limit ends effects [Stansby(1974)]. High velocity is in the bottom side and low velocity in the upper side of the splitter plate. The coordinate system is x in streamwise direction, y in cross-stream (vertical, parallel to the axis of the cylinder) and z in spanwise direction. The origin is taken so that x=0 and z=0 on the cylinder axis and y=0 on the centerline of the trailing edge of the splitter plane.

Results from [Heitz(1999)] have shown a resulting $3D$ complex flow from this configuration. He has demonstrated that the mixing layer generates a marked separation between, on one side, a high velocity wake and, in the other side, a low velocity wake. Each separated wake shows a different drift from the behaviour of a wake in a uniform velocity field at equivalent Reynolds number. So, the cylinder axis direction (y), appears to be a direction of strong inhomogeneity in such a flow. In addition, an instationary secondary flow has been highlighted, going from the low velocity side to the high velocity side of the mixing layer. Measurements and calculations of characteristic magnitudes (C_D, C_p, L_f and S_t) have added evidence that the flow cannot be reduced to a superposition of two uniform wakes. An analogy have been made, on the low velocity side, with an uniformly sheared turbulent flow [Tavoularis *et al.*(1987)] with addition of important ends effects. For the high velocity wake, an analogy was proposed with a wake been modified by the presence of a splitter plate in the near wake.

Simply stating that inhomogeneity arises in a given direction when it is a direction of strong velocity gradient, one can assert that the flow under study is inhomogeneous in all three directions: in streamwise direction x because of the continuous mixing layer expansion, sharply modified by the local velocity deficiency in the wake ; in the cross-flow direction y because of the separation in two different flows under action of the mixing layer velocity gradient and in the spanwise direction z because of the gradients associated with the wake velocity deficiency. This implies that this particular turbulent complex flow is clearly a case where classical POD is liable to provide relevant information on the 3D flow organisation.

3 Proper Orthogonal Decomposition (POD)

[Lumley(1967*a*)] suggests that the Coherent Structures within a randomfield can be identified with the realization of the flow that possesses the largest projection onto the flow field. This approach, the POD, is a classical tool in Probability theory [Loeve(1955)]. This method is also called, among other denominations, Karhunen-Loeve expansion in Pattern Recognition theory [Ash & Gardner(1975), Fukunaga(1972)] or Principal Component Analysis in statistical analysis [Ahmed & Goldstein(1975)].

Compared to many other classical methods used for Large Scale Structure identification (Conditional Methods, VITA, Pattern Recognition Analysis,...), POD is very attractive because no *a priori* is needed for the eduction scheme. Only

a set of flow samples is necessary. From these samples a two-point correlation tensor is constructed for one or several directions (spatial or/and temporal) and for one or several flow variables. Adding directions or variables leads to more complex decompositions but generally leads to more precise description of the Large Scale Structure [Delville(1995)].

Solving the POD problem can be reduced to determining the solutions of an integral eigenvalue problem (Fredholm equation) where the kernel is the correlation tensor. A basis of uncorrelated orthogonal functions (eigenfunctions or eigenvectors), which are characteristic of the most probable "flow realizations" is then obtained. This important property permits the decomposition of every flow realization onto the basis of eigenfunctions obtained. By definition, POD is optimal in terms of the description of the energy present within the flow.

POD consists of searching, for a set of deterministic uncorrelated, flow realizations that correspond to preferred modes $\Phi(X)$ of the flow. Consider $u(X)$ to be a set of realizations of the velocity field ($X = (x, y, z; t)$). To determine these modes it is simply required to search within the flow realizations $u_i(X)$ for the $\Phi(X)$ "closest" in average to this set. At this level, the average is not defined, and will depend on the kind of POD used.

Mathematically this problem can be written:

$$\frac{\langle (u, \Phi)^2 \rangle}{(\Phi, \Phi)} \stackrel{!}{=} Max \quad , \tag{2}$$

where (u, v) corresponds to the scalar product u by v defined by:

$$(u, v) = \int_{\mathcal{D}} u(X)v(X)dX = \sum_{i=1}^{n_c} \int_{\mathcal{D}} u_i(X)v_i(X)dX \quad , \tag{3}$$

Depending on the way the ensemble average $\langle \bullet \rangle$ is defined for calculating the kernel of the integral eigenvalue problem, different orthogonal decompositions can be obtained: classical, snapshot, extended, biorthogonal, ... For example, the ensemble average can consist of:

- a temporal average, under the ergodicity assumption in statistically stationary flows (*"classical" method*); the kernel of the POD problem is then a two-points space correlation tensor (eg with shape $< u(x)u(x') >$)
- a spatial average, estimated for N uniformly sampled discrete times $t_n = n\tau$ for $n = 1, \ldots N$, for which the instantaneous flow fields $u_i(x, n\tau)$ are uncorrelated, where τ is a time scale, characteristic of the correlation time (*"snapshots" method* [Sirovich(1987)]). The kernel is then a two points time correlation tensor (e.g. with shape $< u(t)u(t') >$)

For the same discrete and finite set of data, these two approaches can be shown to be equivalent. Note that most of the time, both for experimental and numerical approaches, a discrete set of N_s spatial nodes obtained at N_t discrete times are available. The choice of a *classical* or *snapshot* approach is then essentially related to computational aspects. In a discrete approach of the POD, the eigenvalue problem to be solved is of rank N_p, the number of grid points. Therefore for applications of POD to computation or PIV experiments, the size of the set of samples being considerably smaller than the number of spatial nodes, the snapshot POD is generally used.

However in the present study, the three spatial directions being strongly inhomogeneous and no experimental way being presently available to get a fully 3D-three components instantaneous description of the flow, a snapshot POD approach is not possible and a 'classical' POD has to be used.

This problem leads to the Fredholm integral eigenvalue problem of equation (1). Practically we solve this problem by considering the following matrix diagonalization problem: find the eigenvectors and eigenvalues of a symmetric definite-positive matrix:

$$A\mathbf{\Phi} = \mathbf{\Lambda\Phi},$$

where A is a discrete representation of the two point velocity cross-correlation tensor. The correlation tensor is obtained from block ensemble average, according to stationarity and ergodicity hypothesis, $R_{ij}(\mathbf{x}, \mathbf{x}') =< u_i(\mathbf{x})u_j(\mathbf{x}') >$, where $\mathbf{x}$=(x, y, z). The structure of A will be discussed in section 5. The eigenvalues, $\lambda^{(n)}$, are representative of the integrated turbulent kinetic energy.

Note that according to the Hilbert-Schmidt theory, solutions of equation(1) could be expressed as :

$$u_i(\mathbf{x}, t) = \sum_n a^{(n)}(t)\Phi_i^{(n)}(\mathbf{x}) \tag{4}$$

with projection coefficients,

$$a^{(n)} = \int_{\mathcal{D}} u_i(\mathbf{x}, t)\Phi_i(\mathbf{x}, t)d\mathbf{x}. \tag{5}$$

However in our case, even if the eigenvectors can be obtained, this projection is not possible, because only partial measurements (two slices from the full domain) are performed at the same time.

The flow studied here is a $3D$ complex flow with no direction of homogeneity (section 2), so the two points correlation tensor have to be supplied for all combinations of positions in the chosen mesh. This leads to a $3D$ correlation tensor of the two first fluctuating velocity components (u',v'). The POD is applied to these two components only and the eigenvectors $\Phi_u^{(n)}$ and $\Phi_u^{(n)}$ are known in the full domain of analysis. Afterwards, the third component of eigen vector ϕ_i is calculated from continuity equation:

$$\Phi_w^{(n)}(x,y,z) = -\int_0^z (\partial\Phi_u^{(n)}(x,y,\eta)/\partial x + \partial\Phi_v^{(n)}(x,y,\eta)/\partial y)\, d\eta \tag{6}$$

In a first step, considering the symmetry condition of the flow in the z direction, we impose $\Phi_w^{(n)}(x,y,z=0) = 0$ making it possible to use equation 6. Finally, a full 3D-three components description of the organisation of the velocity field can be obtained.

4 Experimental setup: $bi - PIV$

Data were acquired from a set of two PIV systems, the two light sheets being placed parallel to each other and independently moved to obtain pairs of instantaneous velocity fields with a varying spatial gap between the measurement planes. Parallel planes were disposed in the vertical xy direction. The study was concentrated on the beginning of the wake, immediately downstream of the cylinder, in order to capture images including the end of the near-wake interaction zone.

Illumination polarized system

The illumination setup was made of two lasers systems Nd.YAG of double-pulses (Quantel and New Wave) (1)(2) with an ouput energy of 30 mJ per pulse at a green wavelength λ=532 nm. It was planned that the velocity correlation tensor could be supplied through a combination of N_z=21 plane positions in xy orientation (see section 5). This led to 231 configurations, with a varying gap between the two light planes. For the smallest values of the distance between the parallel planes, the gap appeared to be smaller than the camera focus length. Moreover we wanted to capture simultaneous velocity fields in the same plane. So, we had to use polarized lights in order to obtain independent images of the seeded flow. The light emitted by the two laser systems were initially polarized in the same direction, each beam being splitted into a thin light sheet (5) (6) (less than 1mm thickness) by a semi-cylindrical lens (7). A mirror (8) was placed across one of the two light sheets in order to change its polarization orthogonally to that of the incident light. By equiping each camera with a polarizing filter corresponding to one light sheet, the system was made able to capture independent images of the flow. In order to verify the efficiency of the polarization system, the two cameras were positioned to see the same single light sheet plane, the other being switched off. The flow was seeded with particles and a video monitor was used to control, in grey levels display, the images recorded. The system yielded a perfect separation, one camera correctly capturing image pairs leading to valid calculations of velocity fields through a cross-correlation treatment by the Dantec PIV system (11) and its Flowmap software (12), while the second camera showed totally black images.

Tracer particles

To get a correct scattering of orthogonally linearly polarized light, an olive oil generator (Ardonceau type) was used. The spray was generated through a Laskin nozzle, feeded with pressurized air, and an impacting plate was used to reduce particles diameter (d). Particles diameter ($dp \approx 1\mu$m) was set greater than the incident light wavelenghth ($0.532\ \mu m$), in order to remain in a configuration where Mie-scattering theory applies [Raffel *et al.*(2000)].

The spray generator was located downstream of the test section (13) in the closed loop of the wind tunnel, to ensure a good homogeneity of the seeding in the view planes.

Image recording system :

The image were captured by two CCD Kodak cameras (type 700) (3) (4), of 768×486 pixel resolution and 8 bit dynamic range. The cameras were placed on both sides of the test section so that the upstream edge of the images correspond to $0.9D$ downstream of the cylinder axis, the image size in physical space being $L_x \times L_y = 84 \times 62$ mm^2. Each individual system, composed of one camera and one laser light sheet emitter, was set on a displacement device moving parallel to the z axis (9) (10). So, for each of the two PIV systems, the focal adjustment was conserved along the whole acquisition procedure, the camera and the light sheet being jointly displaced.

Synchronization and correlation

The lasers pulse rate was adjustable up to 20Hz but the acquisition frequency was limited to 15Hz by the camera frame rate. Synchronization of the cameras aperture with the laser pulses, and synchronazition between the two lasers were achieved under control of the FlowMap hardware (12). Flowmap was also used to calculate the cross-correlation of the two couples of grey level images acquired by the cameras. A 50% overlap of interrogations cells was chosen for the cross correlation calculations (32×32 pixels cells).

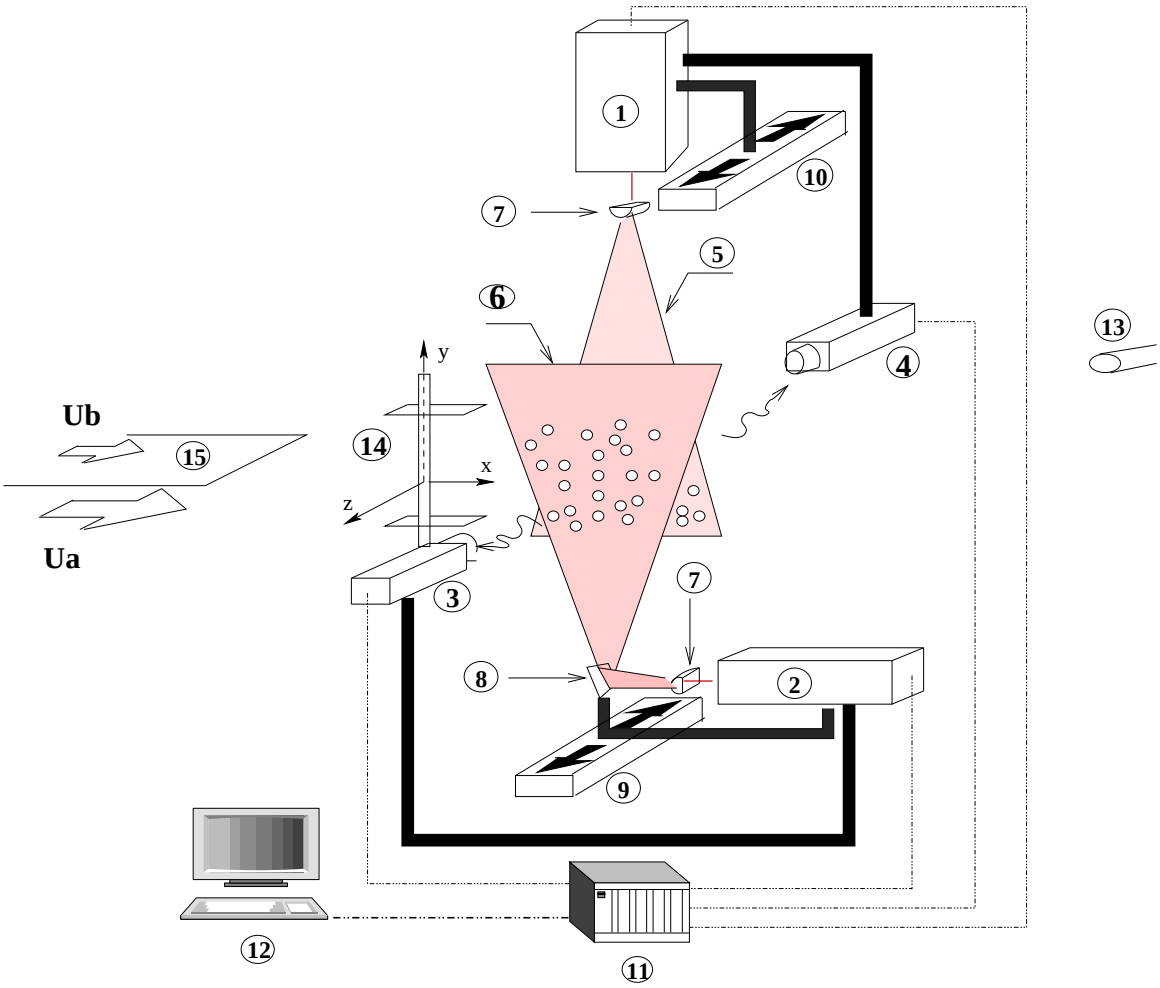

1	Laser emitter Quantel (20 Hz, 2 × 30 mJ)	9 10	displacement system
2	Laser emitter New Wave (20 Hz, 2 × 30 mJ)	11	FlowMap hardware
3 4	CCD cameras (with polarizing filters)	12	Flowmap software
5 6	Laser light sheets	13	Dowstream seeding
7	Laser optic system (semi-cylinder lens)	14	Circular cylinder
8	Mirror	15	Mixing layer splitter plate

Figure 3: Experimental setup

As 231 configurations had to be treated, each one with two PIV planes, it appeared mandatory to reduce post-processing on calculated velocity fields. The vector maps were only submitted to rejection of erroneous vector outside a range of vector norme $|3.7|$ m/s$< U < |36|$ m/s. No other validation method was applied, apart from a classical signal to noise ratio test (peaks < 1.3 were rejected). The resulting validation process led to rejection of less than 1% of the vectors. No filtering was applied to the data before calculation of the correlation tensor.

5 Estimation of the POD Kernel

This section explains how the two point correlation tensor, noted $R_{ij}(\mathbf{x}, \mathbf{x}', t = 0)$ with $\mathbf{x} = x, y, z$ and $\mathbf{x}' = x', y', z'$ is supplied by the experiments (ie. set of two $2D$ PIV planes acquired simultaneously).

3D POD kernel: The PIV planes are set parallel (in a x, y plane), at some spanwise positions noted z for the first PIV plane and z' for the second one. A set of 231 different configurations of this couple of planes (i.e. two simultaneous PIV plane at z and z') with a variable spanwise separation $z - z'$ is acquired. The number of vectors per PIV plane is $N_x \times N_y = 47 \times 29$.

The matrix A is built from blocks (7). Thus, for each vector map couple (i.e. two simultaneous PIV planes at z and z'), a $2D$ two points correlation tensor can be calculated, noted $R_{ij}(X_1, X_2)$ with $X_1 = x, y$ (first PIV plane) and $X_2 = x', y'$ (second PIV plane), for the first two components of the velocity fluctuation (u,v). The block size depends on the number of velocity vectors obtained in each PIV plane (i.e. related to the PIV plane or CCD cameras resolution: $N_{block} = 2 \times N_x \times N_y$):

$$A_{z,z'} = \left(\begin{array}{c|c} R_{uu}(X_1, X_2) & R_{uv}(X_1, X_2) \\ \hline R_{vu}(X_1, X_2) & R_{vv}(X_1, X_2) \end{array} \right)_{z,z'} \tag{7}$$

Each block $A_{zz'}$ can be placed in the full matrix A representing the $3D$ correlation tensor $R_{i,j}(X, X', t = 0)$ with N_z (equal to N'_z) number of positions following the mesh in the spanwise direction (equation (8)) .

$$R_{i,j}(X, X', t = 0) = \left(\begin{array}{c|c|c|c|c} A_{11} & & \dots & & A_{1N_z} \\ \hline & \ddots & & & \\ \hline \vdots & & A_{zz'} & & \vdots \\ \hline & & & \ddots & \\ \hline A_{N'_z 1} & & \dots & & A_{N'_z N_z} \end{array} \right) \tag{8}$$

Finally, the rank of the matrix to be diagonalized for the full $3D$ correlation tensor is $N_{tot} = N_{block} \times N_z$. In the present study, for the mesh used, $N_{tot} = 2 \times 47 \times 29 \times 21 = 56526$ (a rather large rank to handle with!).
Note however that, by considering the blocks[1] and hermitian symmetries[2] of the correlation tensor, it is not useful to estimate the $N_z \times N'_z$ blocks, only the upper triangular part of the matrix A is necessary. That's why only $(N_z + 1) \times N_z/2$ (z, z') configurations are to be studied. In the present study this leads, for a spanwise mesh of 21 locations, to a global number of runs of 231.

2D POD kernel: Considering only one spanwise position (i.e. given couples of two plane PIV for the same $z = z'$), a much smaller $2D$ correlation tensor can be used for a first analysis (the order of magnitude of the problem to be solved being $N_x \times N_y$). In this case, we have to apply independently, for each z location, what we call a *slice POD* that provides a partial description of the flow organisation, not taking into account the spanwise organisation. Note that this approach is a subset of the full 3D problem where only the blocks located on the diagonal of A are considered (i.e. all the blocks involving $z \neq z'$ are put to zero).

[1] $R_{uv}(X1, X2) =< u(x, y).v(x', y') >=< v(x', y').u(x, y) >= R_{vu}(X1, X2)$
[2] $R_{uu}(X_1, X_2) =< u(x, y).u(x', y') >=< u(x', y').u(x, y) >= R_{uu}(X_2, X_1)$ (idem with R_{vv})

6 Comparison of PIV measurements with previous hot wire results

Reminder of the flow parameters :

		[Heitz(1999)]	present work
Cylinder diameter	(D)	15 [mm]	8 [mm]
High velocity	(u_a)	9 [m/s]	18 [m/s]
Low velocity	(u_b)	6 [m/s]	11.7 [m/s]
Reynolds number	$(R_e = U_m D/\nu)$ with $U_m = (u_a + u_b)/2$	7 500	7 920

Before using the $bi - PIV$ measurements for a POD analysis, a preliminary comparison was made with previous hot wire data obtained by [Heitz(1999)], in order to verify that the characteristics of the flow (2) could be retrieved in the PIV measurements. From each series of single PIV xy planes, values of mean velocity and velocity fluctuations were reconstructed in yz planes, in which coherent series of hot wire measurements were available. Partial results for the $x/D = 5.5$ plane are given in Fig. 4. The main topoligical characteristics of the flow could be retrieved from the PIV measurements. As shown in [Heitz(1999)], the cylinder wake is markedly splitted in two different wakes under effect of the mixing layer. The interaction zones, where the wakes and the mixing layer interact, show identical shapes and comparable levels in mean velocity and Reynolds stresses. Some quantitative discrepancies appeare between hot wire and PIV results, mainly in the level of the wake velocity deficiency and of the local velocity gradients. Some weakness can be supposed as regards the ability of PIV to retrieve exact values of local velocity gradients in our case, due to the particle inertial behaviour, but hot wire measurements can also be questioned, especially in regions were high three-dimensionality causes errors in the measurement of the U component with single wire probes. The comparison results were found sufficient to validate the PIV data as correctly describing the topology and dynamical behaviour of the flow.

7 POD results

In this section we first analyse the truncated results obtained from the *slice-POD* approach and then the results obtained from the full 3D POD approach.

7.1 Slice-POD

The main results obtained in this truncated POD, where no spanwise correlation is taken into account, are summarized on Fig. 5.

When the slice is located out of the mixing layer-wake interaction area, the dominant organization is found to be very close to the one that can be observed in a plane mixing layer. The vector fields and iso-$\Phi_u^{(n)}$, plotted on Fig. 5-a) to c) for the first three POD modes obtained at $z/D = -4$, clearly exhibit a large scale organization where large scale vortices appear. The mode 1 and 2 show the same streamwise length scale and are spatially phase shifted : this result is a consequence of the convective nature [Rempfer(1996)] of the flow and the same behaviour could be noticed whatever the slice location was (not shown here). The streamwise length scale λ_x, corresponding to the streamwise distance of two centres of iso-Φ areas with same sign, that can be associated to these two first POD-modes is $\lambda_x \sim 9D$, leading to an equivalent Strouhal number $S = \delta_\omega/\lambda_x = D/\lambda_x \sim 0.11$. This Strouhal number is about half the conventional value that is found in a plane mixing layer. The first two modes of the *slice-POD* are then focusing on structures of twice the size of the ones that could be expected in a conventional plane mixing layer, however modes 3 and 4 (see Fig. 5-c for mode 3) exhibit the right length scale. This behaviour can be explained by the fact that the four first POD modes are found to have an energy very close to each other. However we will see in the following that these two first modes evolve in agreement with the third 3D POD mode and their organisation can be the footprint of the global large scale motion induced by the wake-mixing layer interaction.

When the slice is located in the wake mixing layer interaction area, a very different behaviour can be observed. The vector field and iso-$\Phi_u^{(1)}$, plotted on Fig. 5-d for the first POD mode, obtained at $z/D = -1.25$, show that the spatial organization is quite different. Typical Λ-shape structures are then evidenced. The slant and the streamwise length scale of these structures are different in the high and low velocity sides. This shows that a strong organization is created by the wake-mixing layer interaction. Typical Λ-shape structures are then evidenced. Note that the *average* length scale appearing is of the same order of magnitude than that of the mixing layer (mode 3 of Fig.5-c). The slant and the streamwise length scale of these structures are different in the high and low velocity sides, this last feature will be re-examined and quantified in the following of this paper, after the analysis of the 3D POD results.

7.2 3D POD

For computational reasons, the 3D POD has been solved for a coarser spatial mesh than the experimental one. This mesh is $N_x \times N_y \times N_z = 23 \times 14 \times 17$, leading to $N_{tot} = 10948$. In this POD the spanwise correlations are taken into account and the full 3D organization of the POD modes can be retrieved. A typical example of this 3D reconstruction is illustrated on Fig. 6, where cuts in a horizontal plane ($y = 0$) of the first three eigenvectors are plotted. Clearly modes 1 and 2 exhibit the same streamwise phase shift as noted from the *slice-POD*, traducing once more the mode degeneration due to

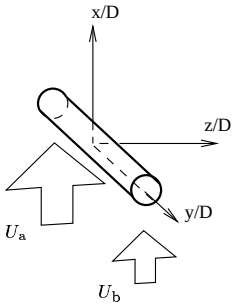

PIV **Hot wire**

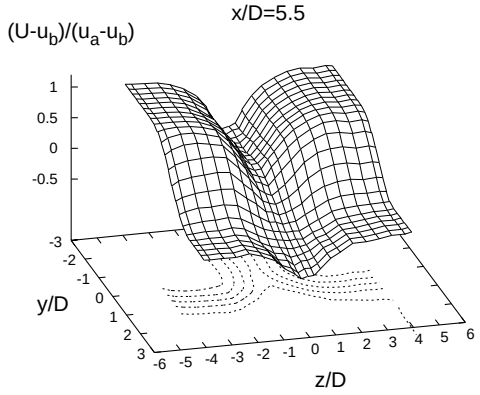

a)

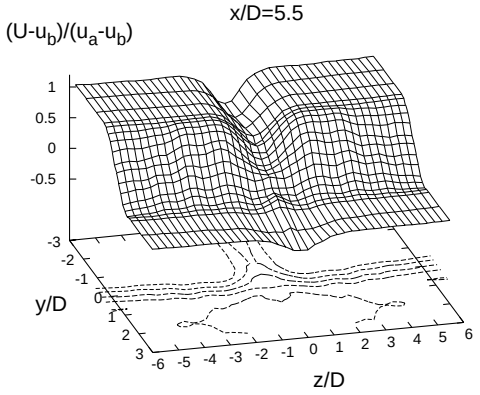

b)

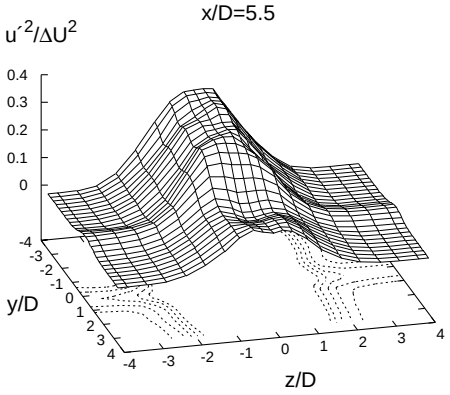

c)

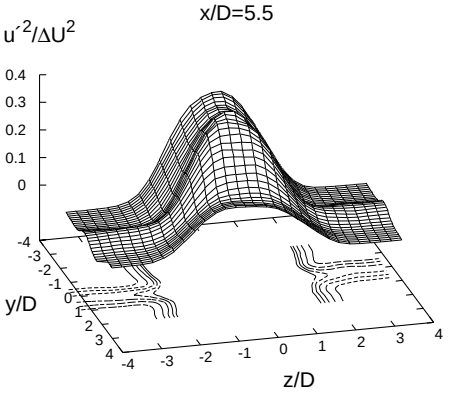

d)

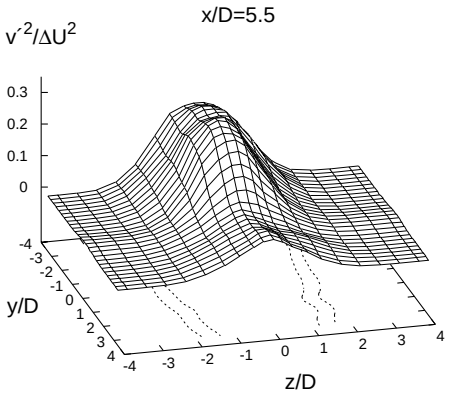

e)

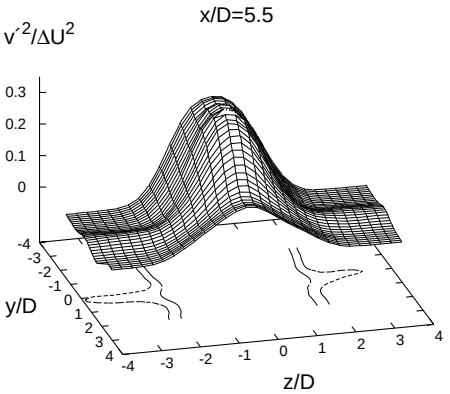

f)

Figure 4: Comparison between PIV and hot wire measurements at $x/D = 5.5$; mean velocity, streamwise component $(\overline{u} - u_b)/(u_a - ub)$ a) PIV b) hot wire (single wire probe) ; Reynolds stresses: $\overline{u'^2}/(u_a - u_b)^2$ c) PIV d) hot wire (4 wires probe), $\overline{v'^2}/(u_a - u_b)^2$ e) PIV f) hot wire (4 wires probe)

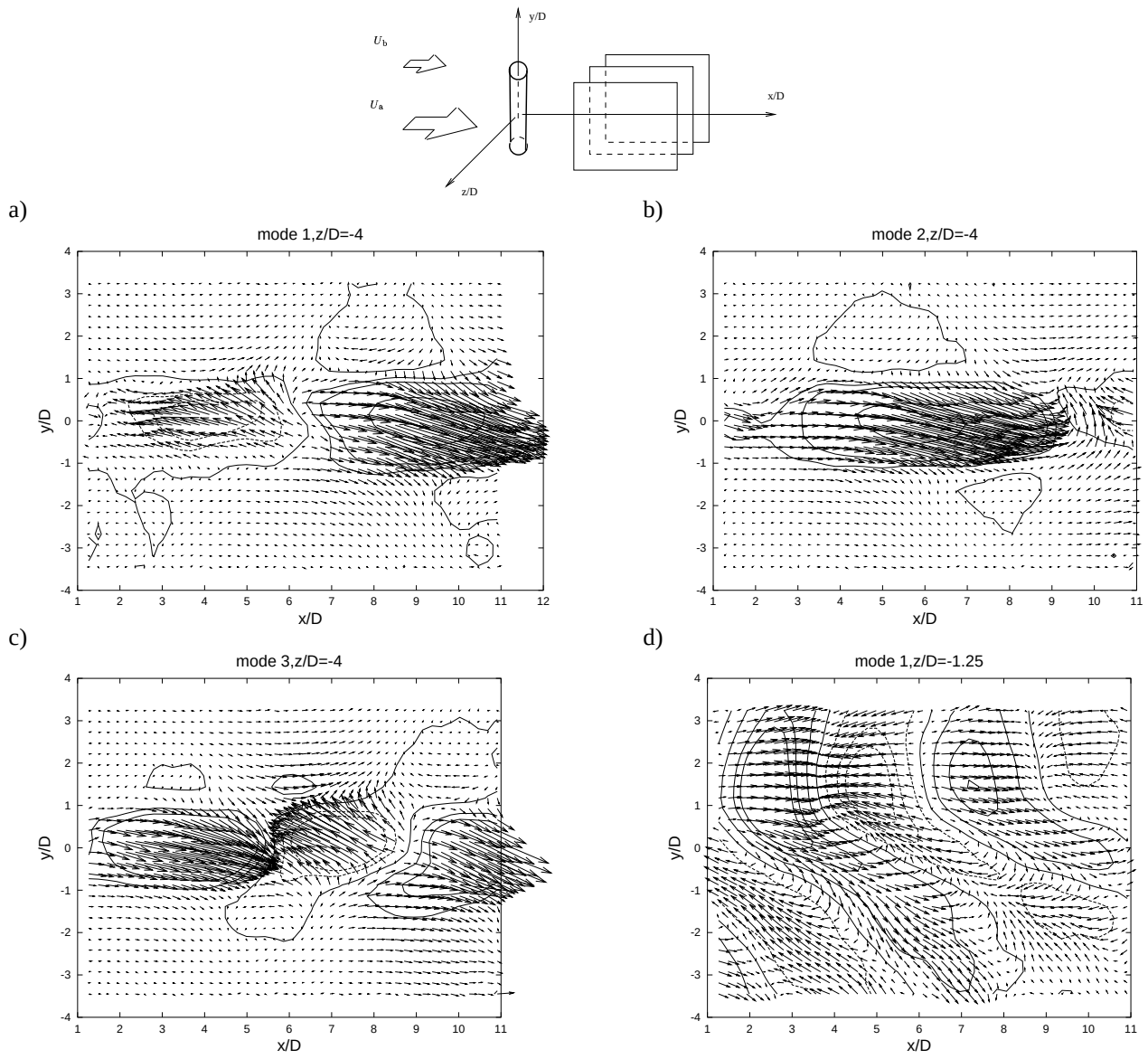

Figure 5: Vector fields in a vertical (x, y) plane corresponding to the contribution of the first *slice-POD* modes for two spanwise locations of the slice. Superimposed on these plots, contours of isovalues of $\sqrt{\lambda}\phi_{uv}/\Delta U$ are drawn (— positive, - - - negative). a)-c) plane located at $z/D = -4$, in the *pure* mixing layer region, a) b) and c) correspond to the first, second and third POD modes respectively ; d) plane located at $z/D = -1.25$, first POD mode in the mixing layer wake interaction zone.

the convective nature of the flow. The overall organization of the first two POD modes is very similar to the one that can be obtained in a conventional wake and corresponds to alternate vortices aligned in the streamwise direction. The spanwise distance between the centres of the counter rotating eddies is closed to D, the cylinder diameter. The longitudinal length scale of this vortices seems to be of the same order of magnitude as the one obtained in the *slice-POD* for mode 3 in the region out of the interaction area (Fig. 5-c), and for mode 1 in the interaction region (Fig. 5-d). On the other hand, mode 3 exhibits a very large scale global motion with a streamwise length scale comparable with that of the first *slice-POD* mode of Fig. 5-a. The topology of this organization corresponds to a focus located at $x/D \sim 6$ and is associated to very high values of vertical velocities corresponding to a rush towards the high velocity side. A more global and qualitative view of the 3D flow organisation is given on Fig. 7-a where isosurfaces of the spanwise vorticity contribution of the first POD mode are shown ($\omega_z = \partial\Phi_v^{(1)}/\partial x - \partial\Phi_u^{(1)}/\partial y$).

This organization can be summarized by considering the schematic view of Fig. 7-b corresponding to the global shape and length scale in a x, y plane, as it can be deduced from the analysis of Fig. 5-d and 7-a. This structures can be modelized as two oblique cells with different angles θ and length scale (λ_θ).

By considering that the effective length scale is the projection $\lambda_0 = \lambda_\theta \cos(\theta)$ [Williamson (1989)] the following results can be obtained:

	angle [°]	streamwise length scale (λ_θ)	*parallel* length scale (λ_0)
Low Velocity side	10	$4.6D$	$3.0D$
High Velocity side	62	$6.6D$	$4.5D$

Logically, the higher frequency corresponds to the high velocity side of the mixing layer (F_{HV}, High Velocity), while the lower frequency is found on the low velocity side (F_{LV}, Low Velocity). The ratio of the *parallel mode* length scales is $\lambda_{0HV}/\lambda_{0LV} \approx 1/r$, r being the velocity ratio $r = U_b/U_a$=0.65 of the mixing layer. It can then be supposed that the *parallel* length scales λ_0, traducing the movement of the oblique cells, are related by the same ratio as the velocity ratio of the mixing layer. This is in good agreement with the behaviour that Williamson observed, when oblique cells were generated by ends effects in the wake of a cylinder. Here, we can suppose that, in a similar way, the mixing layer gives rise to the simultaneous presence of two types of cell arrangements, with two different frequencies, which initiates the propagation of an oblique mode for the cells on both sides.

This analogy with the findings from Williamson is clearly not sufficient to explain thoroughly the cell organization of the coherent structures in that particular flow, since the slope of the structures is growing in the streamwise direction (i.e they tend to bend streamwise), and the wave lengths are varying spanwise. This could be related to the formation of streamwise vortices. When looking at the second POD mode, the structures seem to evolve towards a destructuration on the high velocity side. A more thorough investigation is needed to find whether this is in accordance with the $Yshaped\ cells$ characteristics of the Williamson's second mode of oblique shedding. According to Williamson, that kind of cells is generated by streamwise vortices and is followed by the dislocation of the cells. In the present flow, the "dislocation" of the POD structures might be initiated by the mixing layer which causes the presence of two cells with different frequencies. The analogy with the findings from Williamson have however to be considered with precaution, knowing that Williamson's experiments were mainly constituted by flow snapshot visualizations at low Reynolds (dislocation arising for $R_e < 64$), while the present study deals with much higher Reynolds numbers ($R_e > 7000$), likely to induce other instability modes (mode A and B coming from the three-dimensional effects in the flow [Williamson(1996)]). Furthermore, we must keep in mind that the POD treatment only allows a statistical description of the flow.

8 Conclusion

$bi-PIV$ and POD have been used to underline and analyse the coherent structure organization of the strongly inhomogeneous 3D flow arising from a plane mixing layer impinging a circular cylinder. A polarization technique proved efficient for a full separation of the images captured by two synchronized PIV systems positioned parallel to each other with a varying gap between the two light sheet planes. This permitted the supply of a POD kernel, the resolution of which led to the construction of vector fields corresponding to the successive POD modes. The analysis of the respective contributions from these modes allowed firstly the retrieval of the length scales and frequencies describing the dynamics of the mixing layer and of the two separated wakes on both side of it. The reconstructed fields from both the $slice-POD$ and the $3D-POD$ underlined the presence of oblique cells, probably initiated by the action of the mixing layer on the cylinder wake, in the same way as pointed out by Williamson in his analyse of ends effect on a cylinder wake.

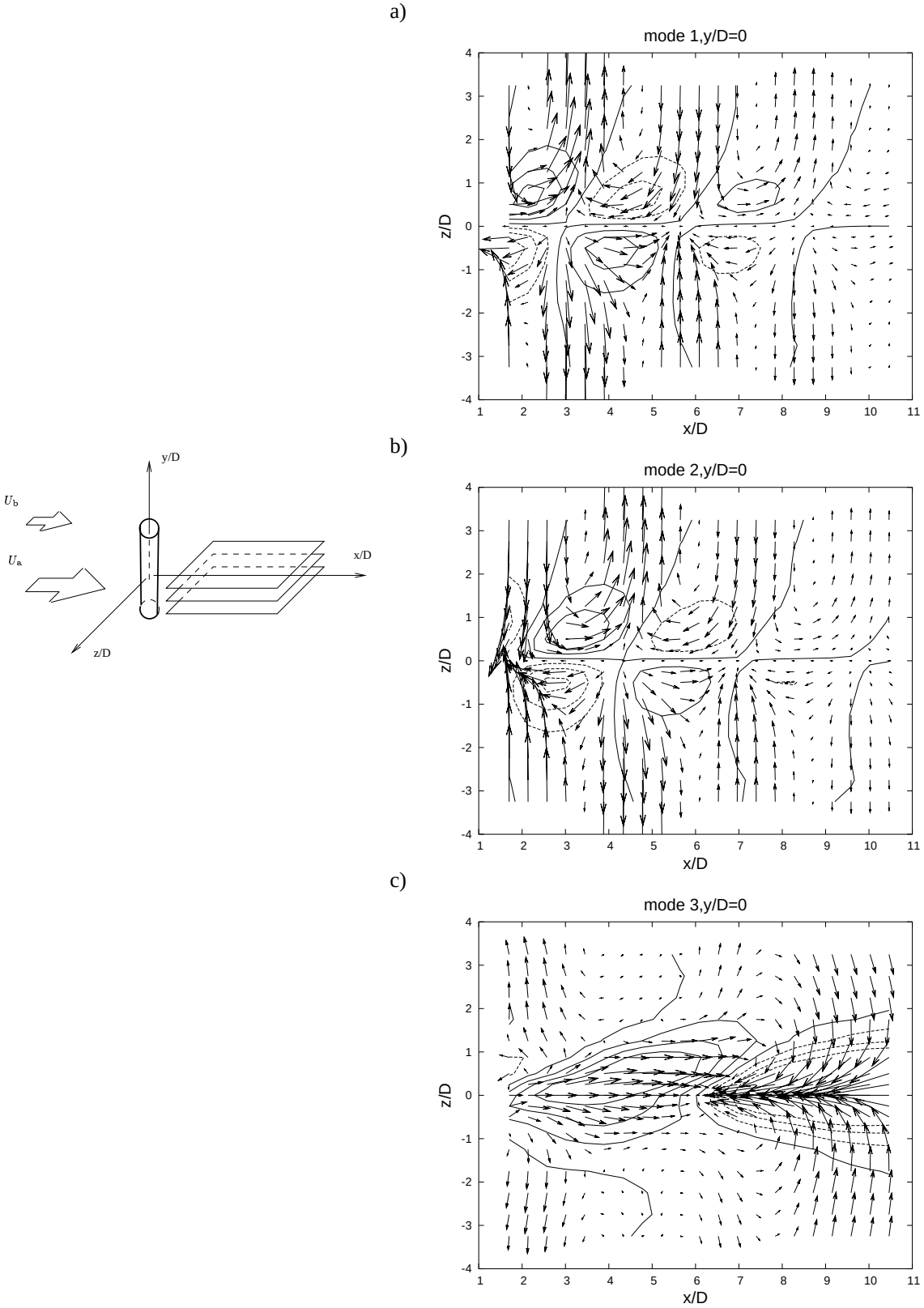

Figure 6: Vector fields in a horizontal (x, z, y=0) plane, corresponding to the contribution of the first 3D-POD modes. Superimposed on these plots contours of isovalues of $\sqrt{\lambda}\phi_{uv}/\Delta U$ are drawn (— positive, - - - negative).

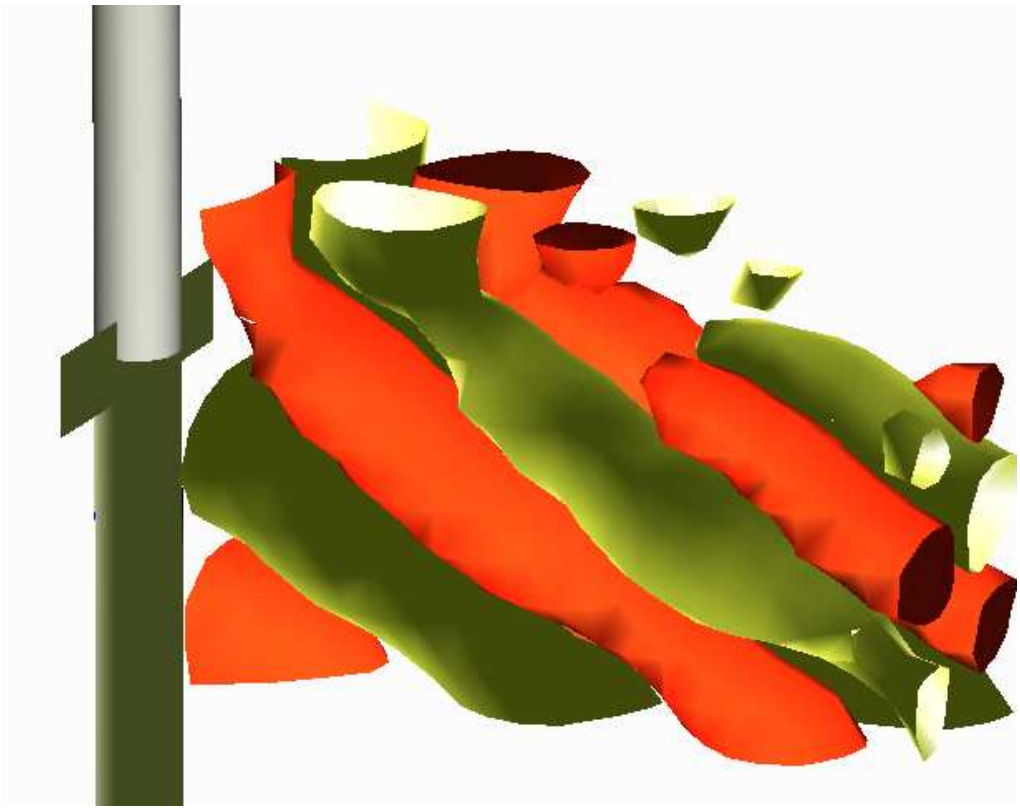

a)

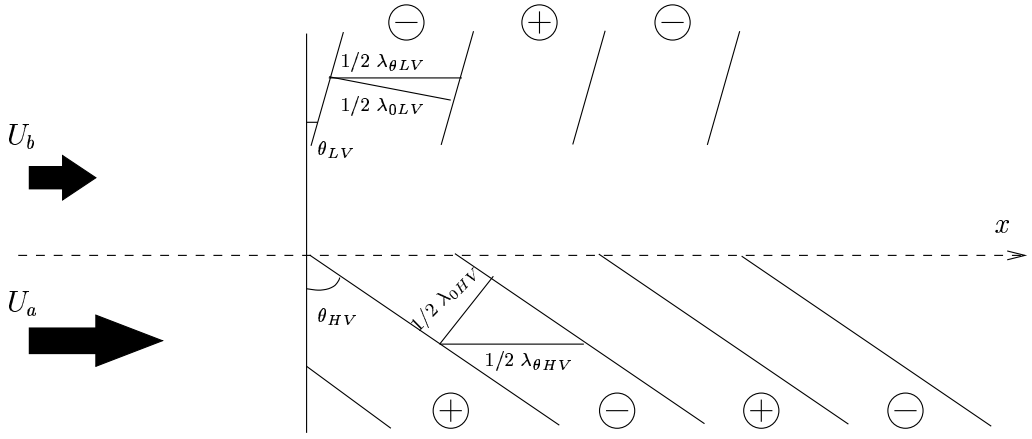

b)

Figure 7: 3D flow organisation. a) Isosurfaces of the spanwise vorticity ω_z contribution of the first POD mode. Plotted are a positive (orange) and a negative (green) isosurfaces ; b) Schematic view of this organisation in a x, y plane.

References

AHMED, N. & GOLDSTEIN, M. (1975) In *Orthogonal transforms for Digital Signal Processing*. Springer-Verlag N.Y.

ASH, R. & GARDNER, M. (1975) In *Topics in stochastic processes*. Academic Press N.Y.

BEARMAN, P. W. (1998) Developments in the understanding of bluff body flows. *JSME International Journal* **41** (1), series B.

DELVILLE, J. (1995) La d´ecomposition orthogonale aux valeurs propres et l'analyse de l'organisation tridimensionnelle des ´ecoulements turbulents cisaill´es libres. PhD thesis, Poitiers university.

FUKUNAGA, K. (1972) In *Introduction to Statistical Pattern Recognition*. Academic Press N.Y.

GASTER, M. (1969) Vortex shedding from slender cones at low reynolds numbers. *J. Fluid Mech.* .

GERICH, D. & ECKELMANN, H. (1982) The influence of end plates and free ends on the shedding frequency of circular cylinder. *J. Fluid Mech.* **122**, 109–121.

HEITZ, D. (1999) Etude exp´erimentale du sillage d'un barreau cylindrique se d´eveloppant dans une couche de m´elange plane turbulente. PhD thesis, Poitiers University.

HEITZ, D., DELVILLE, J., ARROYO, G., GAREM, J.-H., BONNET, J.-P. & MARCHAL, P. (1997) Interaction of the wake of a circular cylinder and a plane mixing layer. In *TSF 11'th*, , vol. 1, pp. 5.1–5.6. Grenoble – France.

HEITZ, D., DELVILLE, J., ARROYO, G., J.-H. GAREM, J.-P. B. & MARCHAL, P. (1998) Turbulent plane mixing layer perturbed by the wake of a circular cylinder. In *Advances in Turbulence VII* (ed. U. Frisch), pp. 309–312. Kluwer Academic Publishers.

HU, H., SAGA, T., KOBAYASHI, T., TANIGUCHI, N. & YASUKI, M. (2001) Dual-plane stereoscopic particle image velocimetry: system set-up and its application on a lobed jet mixing flow. *Exp. in fluids* **31**, 277–293.

KAHLER, C. (2000) Multiple plane stereo piv - recording and evaluation methods. In *EUROMECH 411, Appl. of PIV to tubulence measurements*.

KAHLER, C., STANISLAS, M. & DEWHIRST, T. (2000) Investigation of wall bouned flows by means of multiple plane stereo piv. In *International Symposium on applications of laser techniques to fluid mechanics, stereo PIV*.

VON KARMAN, T. & TSIEN, H. (1945) Lifting line theory for a wing in non–uniform flow. *Q. Appl. Maths* **3** (1).

LEWIS, C. & GHARIB, M. (1992) An exploration of the wake three dimensionalities caused by a local discontinuity in cylinder diameter. *Phys. Fluids A* **4** (1), 104–117.

LOEVE, M. (1955) *Probability Theory*, van nostrand edn.

LUMLEY, J. (1967)*a* The structure of inhomogeneous turbulent flows. In *Atmospheric Turbulence and Radio Wave Propagation* (ed. A. Yaglom & V. Tatarski), pp. 166–178.

LUMLEY, J. (1967)*b The structures of inhomogeneous turbulent flow*. Ed A. M. Yaglom and V.I. Tatarsky, pp. 166-178, nauka,Moscou.

MAULL, D. & YOUNG, R. (1973) Vortex shedding from bluff bodies in a shear flow. *J. Fluid Mech.* **60** (2), 401–409.

NORBERG, C. (1994) An experimental investigation of the flow around a circular cylinder: influnece of aspect ratio. *J. fluid Mech.* **258**, 287–316.

RAFFEL, M., WILLERT, C. & KOMPENHANS, J. (2000) *Particle Image Velocimetry*. Springer.

REMPFER, D. (1996) Investigations of boundary layer transition via galerkin projections on empirical eigenfunctions. *Phys. Fluids* **8** (1), 175–188.

SIROVICH, L. (1987) Turbulence and the dynamics of coherent structures.part 1 :coherent structures. *Quarterly of Applied Mathematics* **XLV 3**, 561–571.

SIROVISH, L. (1989) Chaotic dynamics of coherent structures. *Physica D* **37**, 126–145.

STANSBY, P. (1974) The effect of end plates on the base pressure coefficient of circular cylinder. *R. Aeronaut. J.* **78**, 36–37.

SZEPESSY, S. & BEARMAN, P. W. (1992) Aspect ratio and end plate effects on vortex shedding from circular cylinder. *J. Fluid Mech.* **234**, 191–217.

TAVOULARIS, S., STAPOUNTZIS, H. & KARNIK, U. (1987) Vortex shedding from bluff cylindres in strongly sheared turbulent streams. *Journal of Wind Engineering and Industrial Aerodynamics* **26**, 166–178.

WILLIAMSON, C. H. K. (1989) Oblique and parallel modes of vortex shedding in the wake of circular cylinders at low reynolds numbers. *J. Fluid Mech.* **206**, 579.

WILLIAMSON, C. H. K. (1996) Vortex dynamics in the cylinder wake. *Ann. Rev. Fluid Mech.* **28**, 477–539.

WOO, H., CERMAK, J. & PETERKA, J. (1989) Secondary flows and vortex formation around a circular cylinder in constant–shear flow. *J. Fluid Mech.* **204**, 523–542.